

# Electronic Structure of $\text{La}_{1.85}\text{Sr}_{0.15}\text{CuO}_4$ : Characterization of a Fermi Level Band Crossing

Jason K. Perry and Jamil Tahir-Kheli

*First Principles Research, Inc.*

*8391 Beverly Blvd., Suite #171, Los Angeles, CA 90048*

**Abstract:** We present the results of a new Hubbard model for optimally doped  $\text{La}_{2-x}\text{Sr}_x\text{CuO}_4$ . This model uses parameters derived from BLYP calculations on the cluster  $\text{CuO}_6$ . It explicitly includes the  $\text{Cu } d_{x^2-y^2}$  and  $d_{z^2}$  orbitals, the  $\text{O } p_\sigma$  orbitals, and the apical  $\text{O } p_z$  orbitals. When correlation is properly included in the Hubbard model, we find that there is a crossing of two bands in the vicinity of the Fermi level for the optimally doped superconductor. This crossing rigorously occurs along the  $(0,0) - (\pi/a, \pi/a)$  direction of the 2-D Brillouin zone. The crossing arises due to the overlap of a broad “ $B_{1g}$ ” band dominated by  $\text{Cu } d_{x^2-y^2}$  character and a narrower “ $A_{1g}$ ” band dominated by  $\text{Cu } d_{z^2}$  character. We conclude that optimal doping of  $\text{La}_{2-x}\text{Sr}_x\text{CuO}_4$  and related materials is achieved when the Fermi level coincides with this crossing. At this point, formation of Cooper pairs between the two bands (i.e. inter-band pairing or IBP) leads to superconductivity. Furthermore, using geometric considerations, we extend our conclusions to  $\text{YBa}_2\text{Cu}_3\text{O}_{6+\delta}$  and offer a simple explanation for the seemingly complex behavior of  $T_c$  as a function of doping in this material. This behavior can be understood on the basis of multiple band crossings.

PACS Numbers: 74.70.Vy, 74.65.+n

cond-mat/9711184

*Submitted to Phys. Rev. B.*

## I. Introduction.

Eleven years have elapsed since the discovery of high-temperature copper oxide superconductors.<sup>1</sup> In this work, we focus on the recent suggestion by Tahir-Kheli<sup>2</sup> that superconductivity arises in these materials due to an inter-band pairing mechanism (IBP). That is, Cooper pairing of electrons belonging to two distinct bands may be the cause of superconductivity. Such a proposal is appealing as it readily explains why superconductivity is only observed at very specific doping levels.  $La_{2-x}Sr_xCuO_4$ , for instance, shows an optimal  $T_c$  of 39 K when  $x = 0.15$ , but superconductivity quickly vanishes as the doping level is changed.<sup>3</sup> The IBP theory only requires that two bands cross. Should such a crossing exist, then optimal doping is achieved when the Fermi level coincides with this crossing. Precise doping levels are needed to achieve this.

While such band crossings have not been previously noted by others, we find a crossing to occur in optimally doped  $La_{1.85}Sr_{0.15}CuO_4$  within 0.15 eV of the Fermi level using a simple Hubbard model that includes the effect of electron correlation. The crossing occurs between one band which is dominated by  $Cu d_{x^2-y^2}$  character and a second which is dominated by  $Cu d_{z^2}$  character. Moreover, we find that when the model is empirically adjusted to include missing electronic effects, the crossing can be seen to occur at exactly the Fermi level. As detailed in the accompanying article by Tahir-Kheli,<sup>4</sup> a number of key experimental observations that are otherwise anomalous, such as the temperature dependence of the NMR spin relaxation rates and Knight shifts, the Hall effect, the resistivity, and Josephson tunneling, are easily explained with the resulting band structure and the IBP model.

What follows is a detailed account of how this Hubbard model was developed for  $La_{1.85}Sr_{0.15}CuO_4$ . The resulting band structure is discussed in length. In addition we find that other copper oxide superconducting materials can be understood based largely on geometric constraints. As an example, we offer simple arguments as to why  $YBa_2Cu_3O_{6+\delta}$  appears to show two characteristic  $T_c$ 's over an extended doping range.

## II. Computational Details.

### II.A. Cluster Calculations

Parameters for the Hubbard model were extracted from restricted open-shell density functional calculations on the cluster  $CuO_6$ . These calculations used the gradient corrected BLYP functional<sup>5</sup> with the standard 6-31+G\* basis set<sup>6</sup> on the oxygen atoms and Hay and Wadt's<sup>7</sup> effective core potential and basis set on the copper. All calculations were performed using the Jaguar<sup>8</sup> ab initio electronic structure program on a dual processor 200 MHz Pentium Pro running Linux.

The  $CuO_6$  cluster was embedded in a point charge array of 1364 ions. The ions had the formal charges of +2.000 for  $Cu$ , -1.925 for  $O$ , -2.000 for apical  $O$ , and +2.925 for  $La/Sr$ . The total cluster and point charge array had the  $D_{4h}$  symmetry of the tetragonal unit cell and was 5 unit cells wide (18.940 Å) in the  $a$  and  $b$  directions and 3 unit cells tall (39.618 Å) in the  $c$  direction. Fractional charges were used at the edges. It should be noted that at the low temperatures where superconductivity appears, the crystal shows a  $C_{2h}$  distortion

to an orthorhombic unit cell. This should be a relatively small perturbation, so for the sake of simplicity the higher symmetry structure was used. However, we note here that the distortion will have some important implications in regard to superconductivity. This will be discussed below. The tetragonal crystal structure was taken from Hazen<sup>9</sup> and is given in Table I.

To obtain the Hubbard parameters, the density of a single state was optimized and the resulting orbitals were localized. By then making specific combinations of the localized orbitals and not allowing them to relax in subsequent DFT calculations, it was then possible to determine the Hubbard parameters associated with the localized orbitals. For example, evaluating the energy of the state where there is one hole in the localized  $Cu d_{x^2-y^2}$  orbital ( ${}^2B_{1g} [CuO_6]^{-10}$ ) and using the state where there are no holes at all ( ${}^1A_{1g} [CuO_6]^{-11}$ ) as a reference yields the orbital energy for  $Cu d_{x^2-y^2}$ . Evaluating the energy of the state where there are two holes in the  $Cu d_{x^2-y^2}$  orbital ( ${}^1A_{1g} [CuO_6]^{-9}$ ) then leads to the self-Coulomb term for this orbital. Similarly, evaluating the energy of a state where there is one hole in the plus combination of the localized  $Cu d_{x^2-y^2}$  and  $O p_\sigma$  orbitals as compared to the state where there is one hole in the minus combination of these orbitals leads to the matrix element coupling the two orbitals. Clearly, all principle nearest neighbor Hubbard parameters describing the set of  $Cu$ ,  $O$ , and apical  $O$  orbitals can be obtained in such a fashion using just this single  $CuO_6$  cluster.

The density that was optimized was for the undoped ground state,  ${}^2B_{1g} [CuO_6]^{-10}$ . This state has one hole in an orbital that is about 50%  $Cu d_{x^2-y^2}$  and 50%  $O p_\sigma$ . The state was chosen because it represents the closest approximation to the true density that can be obtained with this finite cluster. Note however that the point charge array reflects a doped state ( $x = 0.15$ ) so the total charge on the system (cluster + point charges) is -0.3. While it was not possible to treat the cluster with a fractional charge to make the total charge on the system neutral, this discrepancy was effectively removed by the procedure described below in section II.B.1.

The orbitals were localized using the Pipek-Mezey<sup>10</sup> localization procedure which maximizes the sum of the squares of the atomic Mulliken populations over basis functions. This procedure was done in several steps. First, orbitals within a given irreducible representation were localized and identified. This produced localized  $Cu d_{x^2-y^2}$  ( $B_{1g}$ ) and  $d_{z^2}$  ( $A_{1g}$ ) orbitals, and symmetry combinations of the  $O p_\sigma$  ( $A_{1g}$ ,  $E_u$ , and  $B_{1g}$ ),  $O p_\pi$  ( $B_{2g}$ ,  $E_u$ , and  $A_{2g}$ ), and apical  $O p_z$  ( $A_{1g}$  and  $A_{2u}$ ) orbitals. The procedure was then used on the symmetry combinations of the oxygen orbitals to obtain completely localized  $O p_\sigma$ ,  $O p_\pi$ , and apical  $O p_z$  orbitals.

Hubbard parameters were derived by evaluating the DFT energies with fixed orbitals (*i.e.* non-SCF) as follows:

- 1) The energy of the  ${}^1A_{1g} [CuO_6]^{-11}$  state (having no holes) was evaluated. This was used as our reference state.
- 2) The energies of the doublet  $[CuO_6]^{-10}$  states (each having a single hole in one of the localized orbitals) were evaluated. This yielded the orbital energies,  $E_i^0$ .

- 3) The energies of the singlet  $[CuO_6]^{-9}$  states (each having two holes in one of the localized orbitals) were evaluated. This yielded the self-Coulomb repulsion energies,  $J_{ii}$ .
- 4) The Hartree-Fock energies of the triplet and open-shell singlet  $[CuO_6]^{-9}$  states (each having two holes in different localized orbitals) were evaluated. This yielded the exact exchange energy between orbitals,  $K_{ij}$ .
- 5) The energies of the triplet  $[CuO_6]^{-9}$  states (each having two holes in different localized orbitals) were evaluated. This yielded the Coulomb repulsion energy between orbitals,  $J_{ij}$ .
- 6) The energies of the doublet  $[CuO_6]^{-10}$  states (each having one hole in either the plus or minus combination of pairs of localized orbitals) were evaluated. This yielded the matrix elements coupling pairs of orbitals,  $T_{ij}$ . Note that the fully symmetric combinations of the oxygen orbitals were used in the evaluation of these terms rather than the completely localized orbitals.

Parameters obtained from this procedure are listed in Table II. This parameter set will be referred to as the unscaled set.

The Hubbard model that was developed included explicitly the  $Cu$   $d_{x^2-y^2}$  and  $d_{z^2}$  orbitals, the  $O$   $p_\sigma$  orbitals (two per unit cell), and the apical  $O$   $p_z$  orbitals (two per unit cell). This led to a total of six bands. Solving the Hubbard model was done in two parts. The first took the input parameters (orbital energies and coupling terms) and found the single electron energies  $\epsilon_n(k)$  and wavefunctions  $\phi_n(k)$  where  $n$  is the band index. These  $k$  states were filled to the required doping level and the orbital occupations were evaluated. In the second step, these orbital occupations were used to reevaluate the orbital energies. The procedure was repeated until self-consistency was achieved. The Hubbard model is explained in more detail in the accompanying article.<sup>4</sup>

The Hubbard model was solved assuming no dispersion in the  $z$  direction. In calculating the density of states, however,  $z - axis$  dispersion was included perturbatively by assuming a dominant coupling through the apical  $O$   $p_z$  orbitals. Further details follow.

## II.B. Orbital Energy Evaluation

### II.B.1. Coulomb Potential

When orbital occupations are evaluated in the diagonalization step, the change in the Coulomb field had to be incorporated into the orbital energies,  $E_i$ . This is done by dividing up this field into that due to the  $CuO_6$  cluster and that due to the point charge array. Since the reference orbital energies,  $E_i^0$ , were originally defined for the case in which all  $CuO_6$  orbitals were doubly occupied ( $^1A_{1g}$   $[CuO_6]^{-11}$ ), the change in the orbital energies ( $E_i$ ) due to the change in the occupation of the  $CuO_6$  orbitals ( $N_i$ ) were determined from,

$$E_i = E_i^0 - (2 - N_i)J_{ii} - \sum_{j \neq i} (2 - N_j)(J_{ij} - \frac{1}{2}K_{ij}), \quad N_i > 1 \quad (1)$$

$$E_i = E_i^0 - J_{ii} - \sum_{j \neq i} (2 - N_j) (J_{ij} - \frac{1}{2} K_{ij}), \quad N_i \leq 1 \quad (2)$$

where the  $Cu$   $d_{x^2-y^2}$  and  $d_{z^2}$  orbitals, the four  $O$   $p_\sigma$  orbitals and the two apical  $O$   $p_z$  orbitals of the  $CuO_6$  cluster were included in the summation.

The Coulomb potential due to the changing long range field was evaluated by first subtracting off the potential due to the 1364 ion point charge array used in the DFT calculations. This was evaluated as a classical point charge Coulomb interaction at each of the  $Cu$ ,  $O$ , and apical  $O$  sites of the  $CuO_6$  cluster. A similar Coulomb interaction was evaluated with a larger array having 22374 ions (17 unit cells wide in the  $a$  and  $b$  directions (64.396 Å) and 5 unit cells tall in the  $c$  direction (66.030 Å)). This was done to improve the long range Coulomb field over that which was used in the cluster calculations. This new Coulomb field was also broken up into components due to the  $Cu$ ,  $O$ , apical  $O$ , and  $La/Sr$  sites. These fields were then appropriately scaled based on the orbital occupations from the Hubbard model and the effect was incorporated into the new orbital energies.

### II.B.2. Correlation

An important point should be made here about the effect of correlation. As can be seen in equations (1-2), the self Coulomb interaction ( $J_{ii}$ ) is treated separately from the other Coulomb interactions. This is a deviation from the mean field approximation of Hartree-Fock theory and conventional LDA band structure calculations. The mean field approximation would instead use the orbital energy correction equation:

$$E_i = E_i^0 - \sum_j (2 - N_j) (J_{ij} - \frac{1}{2} K_{ij}) \quad (3)$$

While equation (3) may be adequate for many materials, it breaks down in the limit of weakly interacting particles where the self Coulomb terms are much larger than the coupling matrix elements ( $J_{ii} \gg T_{ij}$ ). As can be seen from the data in Table II, this is the case for  $La_{1.85}Sr_{0.15}CuO_4$ . In this regime, equations (1-2) become valid. The difference between equations (1-2) and (3) can be seen when one orbital is at half occupancy ( $N_i = 1$ ). In equation (2) the orbital energy is lowered by the full  $J_{ii}$  term while in equation (3) the orbital energy is only lowered by  $(J_{ii} - \frac{1}{2} K_{ii})$  or equivalently  $\frac{1}{2} J_{ii}$ . Equations (1-2) assumes that correlation localizes all spins, while equation (3) inappropriately assumes the system has ionic character. With equation (3) there is a tendency to completely empty a band before electrons are removed from a second band in order to minimize the self-Coulomb energy. With the proper treatment of  $J_{ii}$  in equations (1-2) there is instead a tendency to remove electrons from multiple bands in order to minimize the Coulomb repulsions between different orbitals.

Variations on the type of correlation expressed in equations (1-2) have been introduced by several authors<sup>11,12</sup> in studies of  $La_2CuO_4$ . Application of the self-interaction correction, or equivalently spin-polarization, has been successful in describing the antiferromagnetic

state of this material. As will be seen in this work, the introduction of correlation through equations (1-2) is critical to obtaining a band crossing in  $La_{1.85}Sr_{0.15}CuO_4$ .

### II.B.3. Orbital Relaxation

Perhaps the main limitation in the method used here to obtain the Hubbard parameters is that the orbitals were not allowed to relax for different states. This will result in Coulomb interactions which are too high and orbital energies which are too low. To determine the effect that orbital relaxation would have on our Hubbard parameters, we looked at isolated  $Cu$ ,  $O$ , and apical  $O$  atoms in the full point charge array. We derived orbital energies and Coulomb interactions for these lone atoms using both fixed orbitals and fully optimized orbitals. The Coulomb energies were found to uniformly scale as 0.7 when relaxation was introduced. The orbital energies (defined here as  $E(\phi^2) - E(\phi) - J_{jj}$ ) did not scale quite as uniformly, so different scales were used for  $Cu$ ,  $O$ , and apical  $O$ . We found that the orbital energy for  $Cu$  scaled as 0.6, for  $O$  as 0.8, and for apical  $O$  as 0.7. We applied all these scales to the Hubbard parameters listed in Table II to produce the set listed in Table III. It is this corrected set that was used in our final calculations. We should point out that we experimented with some other scaled sets (such as that obtained from uniformly scaling both the orbital energies and Coulomb terms by 0.7) and found no qualitative changes in the band structure. Even when the unscaled set was used, the same basic features were still observed.

### III. Results.

In Figure 2 we show the 2-D dispersion of the top two bands as obtained with our Hubbard model using the scaled parameter set of Table III. The band structure was computed for optimally doped  $La_{2-x}Sr_xCuO_4$ , where  $x = 0.15$ . This doping level corresponds to the removal of a total of 1.15 electrons per unit cell from the  $Cu/O$ /apical  $O$  bands (undoped  $La_2CuO_4$  has 1 electron per unit cell removed from these bands). The orbital energies and occupations that were computed self-consistently from the model are given in Table IV.

As can be seen in Figure 2, two bands appear to be important near the Fermi level. While no holes have been created in the lower band the Fermi level is just 0.035 eV above the top of this band. More importantly, a rigorous crossing, which is critical to the proposed theory, is seen just 0.153 eV below the Fermi level along the  $(0,0) - (\pi/a, \pi/a)$  symmetry line (note, there are actually four crossing points in the full 2-D Brillouin zone at  $(k,k)$ ,  $(k,-k)$ ,  $(-k,k)$ , and  $(-k,-k)$ ). The close proximity of this crossing to the Fermi level, as determined from this simple model, is a significant finding. Given errors in the Hubbard parameters and missing electronic effects, it is not difficult to conclude at this point that a band crossing, required of the IBP model, indeed appears to occur at the Fermi level of the optimally doped superconductor. This crossing can be characterized as arising between a broad “ $B_{1g}$ ” band dominated by  $Cu d_{x^2-y^2}$  character and a narrower “ $A_{1g}$ ” band dominated by  $Cu d_{z^2}$  character.

As shown in Figure 3, it is clearly the case that this band crossing is only observed when the self-Coulomb term is treated properly. Using the mean-field equation (3) we find

only a single isolated band having “ $B_{1g}$ ”  $Cu d_{x^2-y^2}$  character at the Fermi level. Other bands are well buried. We clarify this by noting that ligand field theory properly predicts that the  $Cu d_{x^2-y^2}$  orbital is the most unstable and  $d_{z^2}$  is the next most unstable in the Jahn-Teller distorted octahedron of  $CuO_6$ . The highest energy band orbitals of our Hubbard model reflect that this is true. However, as electrons are removed from the  $d_{x^2-y^2}$  orbital the energy of this orbital stabilizes with respect to the  $d_{z^2}$  orbital as a result of reduction in the self-Coulomb energy. This makes it more favorable to remove electrons from the  $d_{z^2}$  orbital. Conversely, as electrons are removed from the  $d_{z^2}$  orbital the energy of this orbital stabilizes with respect to the  $d_{x^2-y^2}$  orbital. Yet because the self-Coulomb energy of the  $d_{z^2}$  orbital is smaller than that of the  $d_{x^2-y^2}$  orbital due to  $s - d_{z^2}$  hybridization, it is actually possible to remove *more* electrons from the  $d_{z^2}$  orbital than the  $d_{x^2-y^2}$  orbital. Such considerations are important since they lead directly to the observed band crossing.

To take our calculations one step further, we considered what electronic effects might be missing that would have the greatest effect on the position of the crossing point relative to the Fermi level. Besides errors that might be present in the basic Hubbard parameters due to basis set limitations, cluster size, and the DFT method itself, a number of missing key electronic effects can be identified. All are expected to lead to only minor perturbations of the band structure, but their cumulative effect could have an impact on the position of the band crossing. These effects include:

- 1) Explicit inclusion of z-axis dispersion instead of the perturbative approach taken here.
- 2) Inclusion of additional Hubbard parameters. Additional parameters should all be  $< 0.04$  eV.
- 3) Explicit inclusion of other bands. Small mixings with other bands, in particular the  $Cu d_{xy}/O p_\pi$  band, could have an effect on the position of the crossing.
- 4) Use of more realistic charges in the cluster calculations.
- 5) Inclusion of additional spin correlation. The current model only includes the self-interaction correction to account for the tendency of weakly interacting systems to localize spin. However, spin couplings between different orbitals, in particular the triplet coupling between  $Cu d_{x^2-y^2}$  and  $d_{z^2}$ , has been ignored.
- 6) Explicit inclusion of the  $La$  and  $Sr$  ions. The current model treats these atoms as point charges having the formal charges  $+3.0$  and  $+2.0$ , respectively. In reality, these ions are likely less highly charged. They also have spatial extent which leads to Pauli repulsions.
- 7) Inclusion of the orthorhombic distortion. The crystal in the superconducting phase is distorted from its high symmetry tetragonal ( $D_{4h}$ ) structure to a lower symmetry orthorhombic ( $C_{2h}$ ) structure.<sup>9</sup> This is manifested by a tilting of the  $CuO_6$  units or equivalently a buckling of the  $CuO_2$  planes. An important effect from this distortion is that two of the four crossing points (at  $(k, -k)$  and  $(-k, k)$ ) become strictly avoided due to the reduced symmetry. However, it should be stressed that the other two crossing points (at  $(k, k)$  and  $(-k, -k)$ ) are maintained, which is critical to the proposed IBP theory.

While it is not clear that all of these effects will be favorable in terms of moving the band crossing toward the Fermi level, their combined effect could easily lead to such a change. We stress that a perturbation of only 0.153 eV (a small quantity on the chemical scale) is necessary to observe a Fermi level crossing.

We have, in fact, applied a specific perturbation to our model in order to incorporate one of the above effects. Investigations of the effect of *La* and *Sr* using a variety of clusters at the BLYP level showed significant mixing of the *O*  $p_\pi$  orbitals with the orbitals of these metals. The implication of these results is that there is diffusion of the *O*  $p_\pi$  electrons onto the *La/Sr* sites which has been ignored by the *CuO*<sub>6</sub> cluster calculations. The effect of this charge diffusion is to lower the energy of both the *O*  $p_\sigma$  and *O*  $p_\pi$  orbitals and raise the energy of the apical *O*  $p_z$  orbitals relative to the *Cu* orbitals. To account for this effect we included in our Hubbard model calculations an adjustable parameter which defined the extent of charge transfer from *O*  $p_\pi$  to *La/Sr*. While we do not explicitly include these  $\pi$  bands in the final model, Coulomb terms for the *O*  $p_\pi$  orbitals were evaluated and included in Tables II and III (*La* and *Sr* were still treated as classical point charges). This allowed us to include the effect of charge transfer by altering the Coulomb field in a fashion similar to that explained in section II.B.1. Orbital energies were reevaluated to reflect the change in the Coulomb field due to this charge transfer.

The primary effect of this charge transfer is to stabilize the  $\pi$  bands relative to the Fermi level by significantly lowering the orbital energy of *O*  $p_\pi$ . A secondary effect, however, is to raise the crossing point of the two bands of interest closer to the Fermi level for the optimally doped system. This was accomplished when the charge transfer term was empirically adjusted to the value of 0.50 electrons transferred. That is, the charge on the *La/Sr* sites was +2.425 compared to the formal charge of +2.925. This should be considered within the range of reasonable charges for these ions (note the charges on the other atoms are +1.563 for *Cu*, -1.429 for *O*, and -1.777 for apical *O*). We should note though, that the extent of charge transfer calculated here may be an overestimate in light of the fact that the other electronic effects listed above have not yet been incorporated. But, as detailed in the accompanying article by Tahir-Kheli,<sup>4</sup> the resulting band structure proves to have the necessary features to explain a number of key experiments.

The 2-D dispersion of the top two bands from these calculations is shown in Figure 4 and the optimized orbital energies and occupations are given in Table V. In addition the Fermi surfaces are shown in Figure 5 and the density of states of the top two bands is shown in Figure 6.

## IV. Discussion.

### IV.A Band Structure of $\text{La}_{1.85}\text{Sr}_{0.15}\text{CuO}_4$

The band crossing we observe arises from the following considerations. In this discussion, we will refer to the two bands that cross as the “ $B_{1g}$ ” and “ $A_{1g}$ ” bands. The crossing produces two new bands that touch, referred to as  $U(\text{pper})$  and  $L(\text{ower})$ . The dispersion of the “ $B_{1g}$ ” band, dominated by *Cu*  $d_{x^2-y^2}$  character, is rather broad, on the order of 2 eV,



producing a low density of states. The dispersion of the “ $A_{1g}$ ” band, dominated by  $Cu d_{z^2}$  character, is in contrast rather narrow, on the order of 0.3 eV, producing a high density of states. At the  $(\pi/a, \pi/a)$  point, the higher energy band is “ $B_{1g}$ ” in nature, corresponding to the completely antibonding combination of  $Cu d_{x^2-y^2}$  and  $O p_\sigma$  orbitals. The lower energy band is “ $A_{1g}$ ” in nature, corresponding to the antibonding combination of the  $Cu d_{z^2}$ ,  $O p_\sigma$ , and apical  $O p_z$  orbitals. At the  $(0,0)$  point, however, the higher energy band is “ $A_{1g}$ ” in nature and the lower energy band is “ $B_{1g}$ ”. Due to this change in the relative energetics between the top of both bands and the bottom of both bands, the “ $B_{1g}$ ” and “ $A_{1g}$ ” bands must cross, producing a  $U$  band and  $L$  band which each have both “ $B_{1g}$ ” and “ $A_{1g}$ ” character. This crossing of bands is strictly avoided everywhere except for one point in the 2-D Brillouin zone. Along the  $(0,0) - (\pi/a, \pi/a)$  symmetry line, the crossing is rigorously allowed since the “ $B_{1g}$ ” and “ $A_{1g}$ ” orbitals cannot mix along this direction. Due to this rigorous crossing, the  $U$  band and  $L$  band must touch. While the position of this crossing point (or touching point) is subject to variation, its existence is quite robust over a wide range of model parameters.

In the closeup of the density of states shown in Figure 6, it can be seen how the crossing of the “ $B_{1g}$ ” and “ $A_{1g}$ ” bands affects the nature of the  $U$  and  $L$  bands. The  $U$  band starts at +0.47 eV and represents the  $(\pi/a, \pi/a)$  point of the “ $B_{1g}$ ” band. The density of states of this band remains consistently low until about +0.10 eV where there is a sharp peak. This peak represents the change in character of the band from “ $B_{1g}$ ” to “ $A_{1g}$ ” in the vicinity of the  $(\pi/a, 0)$  point. The density of states of the  $U$  band remains relatively high at energies below this point, being dominated by “ $A_{1g}$ ” character. The band terminates at -0.25 eV, which represents the  $(0,0)$  point of the “ $A_{1g}$ ” band. The onset of the  $L$  band is characterized by a sharp peak in the density of states at +0.03 eV. This peak occurs in the vicinity of the  $(\pi/a, \pi/a)$  point of the “ $A_{1g}$ ” band. The peak comes down to a low density of states near the Fermi level and the density of states remains low, being dominated by “ $B_{1g}$ ” character until about -0.20 eV when character from other orbitals (in particular the “ $A_{2u}$ ” antibonding combination of the apical  $O p_z$  orbitals) starts to mix in. The change in character of this band at lower energies should have no effect on the issue of the band crossing or the IBP model.

The character of these bands can be seen more clearly in Figure 7. In Figure 7a, the  $U$  band is shown to be dominated by  $Cu d_{x^2-y^2}$  character above 0.10 eV while the  $L$  band is dominated by  $d_{x^2-y^2}$  below the Fermi level. In Figure 7b, the  $U$  is shown to be dominated by  $Cu d_{z^2}$  character below 0.10 eV while the  $L$  band is dominated by  $d_{z^2}$  only at the Fermi level.

While most band structure calculations have only shown a single band at the Fermi level,<sup>13</sup> we argue that this is due to the lack of correlation. In fact, the work of Shiraishi, *et al.*,<sup>11</sup> which included the effect of spin-polarization, found that doping of  $La_2CuO_4$  resulted in the formation of two types of holes from two distinct bands. While no band crossing was noted, the two types of holes were characterized as being  $Cu d_{x^2-y^2}$  and  $d_{z^2}$ . Eto, *et al.*<sup>14</sup> also suggested the importance of the  $Cu d_{z^2}$  orbital based on cluster model calculations. We

find that this work lends support to the findings reported here.

#### IV.B. Band Structure of Related Materials

Certain qualitative features in the density of states for  $La_{2-x}Sr_xCuO_4$  (*LASCO*) should be characteristic of many superconducting copper oxide materials, such as  $YBa_2Cu_3O_{6+\delta}$  (*YBCO*),  $Bi_2Sr_2Ca_{n-1}Cu_nO_{2n+6+y}$ ,  $Tl_2Ba_2Ca_{n-1}Cu_nO_{2n+4+\delta}$ , and others. Each should be characterized by a peak in the  $U$  band just above the top of the  $L$  band. This is due to band repulsions away from the  $(0,0) - (\pi/a, \pi/a)$  diagonal which introduce “ $A_{1g}$ ” character into the  $U$  band. When these band repulsions are large enough (such as they are at  $(\pi/a, 0)$ ), the peak in the density of states of the  $U$  band should occur above the top of the  $L$  band. The  $L$  band, on the other hand, should have a sharp peak at its onset at  $(\pi/a, \pi/a)$  which vanishes as the band becomes “ $B_{1g}$ ” in character.

Although the electronic structure of *YBCO* should share common features with *LASCO*, it differs in one important regard: the local symmetry of *YBCO* in the superconducting state is  $D_{2h}$  as compared to  $C_{2h}$  for *LASCO*.<sup>9</sup> This symmetry will not allow a rigorous crossing of the two bands along the diagonal (or any other point) in the 2-D Brillouin zone. However, it should be recognized that the dual  $CuO_2$  planes of *YBCO* lead to four bands in contrast to the two bands of *LASCO*. Dispersion of these four bands in the  $z$  direction leads to two bands having “ $A_g$ ” symmetry at  $k_z = 0$  and  $k_z = \pi/c$  and two bands having “ $B_{1u}$ ” symmetry. The two “ $A_g$ ” bands are principally composed of the bonding combinations of the  $Cu d_{x^2-y^2}$  orbitals from the two planes and the bonding combinations of the  $Cu d_{z^2}$  orbitals from the two planes. The “ $B_{1u}$ ” bands are the antibonding analogues. While the two “ $A_g$ ” bands are not precluded from mixing at any symmetry point, and the two “ $B_{1u}$ ” bands are also not precluded from mixing, the “ $A_g$ ” and “ $B_{1u}$ ” bands cannot mix when  $k_z = 0$  or  $k_z = \pi/c$ . This suggests that crossings could occur between the “ $A_g$ ” bands and the “ $B_{1u}$ ” bands. Based on this idea, we propose the following scenario. (Note, we do not address the effects of the chain  $CuO$  bands. These bands will perturb the planar  $CuO_2$  bands, but we suspect the essential topology described below holds.)

There are two sets of two bands ( $U$  and  $L$ ) having qualities similar to those shown here for *LASCO*. One set has “ $A_g$ ” symmetry while the other has “ $B_{1u}$ ” symmetry. The primary difference between these bands and those of *LASCO* is that the crossing along the  $(0,0) - (\pi/a, \pi/a)$  direction is avoided. Since the  $Cu d_{x^2-y^2}$  dispersion in the  $z$  direction is expected to be small, the  $d_{x^2-y^2}$  components of these bands (analogous to the “ $B_{1u}$ ” bands of *LASCO*) should be nearly degenerate. In contrast, the  $Cu d_{z^2}$  components of these bands (analogous to the “ $A_{1g}$ ” bands of *LASCO*) should be separated in energy.

The onset of superconductivity in *YBCO* should occur when the Fermi level coincides with a band crossing. This likely occurs at  $k_z = \pi/c$  between the “ $B_{1u}$ ”  $L$  band (which is completely antibonding in the  $z$  direction) and the “ $A_g$ ”  $U$  band. Interestingly, it is not required to occur along the  $(0,0) - (\pi/a, \pi/a)$  direction. In fact, there is likely a double crossing within a quadrant of the Brillouin zone, as depicted in Figure 8. In this schematic, we view the Fermi surfaces as squared circles centered around  $(0,0)$  for “ $B_{1u}$ ”  $L$  and “ $A_g$ ”

$L$  and centered around  $(\pi/a, \pi/a)$  for “ $B_{1u}$ ”  $U$ . Superconductivity begins when the “ $A_g$ ”  $L$  and “ $B_{1u}$ ”  $U$  bands first touch. Since the radius of the “ $B_{1u}$ ”  $U$  Fermi surface is increasing faster than the radius of the “ $A_g$ ”  $L$  Fermi surface is decreasing (due to the difference in their densities of states), two crossing points can be sustained over a wide doping range. At sufficiently higher doping levels, a second set of band crossings of a similar nature should occur at  $k_z = 0$ . This proposal easily explains the extended doping range observed for  $YBCO$  and the appearance of two  $T_c$ ’s in different doping regimes for this material. Furthermore, it suggests a reason for the increasing  $T_c$  for  $LASCO$  vs. underdoped  $YBCO$  vs. optimally doped  $YBCO$ . We correlate an increase in the number of crossing points, or, more correctly, the number of crossing points which are thermally accessible, to an increase in  $T_c$ . Indeed, it is observed that superconductivity begins with  $YBa_2Cu_3O_{6.6}$  showing a  $T_c$  of 60 K. This  $T_c$  is sustained upon further doping until a rapid increase to  $T_c = 90$  K is observed near  $YBa_2Cu_3O_{6.9}$ . Further doping to  $YBa_2Cu_3O_{7.0}$  maintains  $T_c$  at this higher temperature.<sup>15</sup>

Similar analysis can be applied to the bismuth<sup>16</sup> and thallium<sup>17</sup> systems. We note that in these systems an increase in  $T_c$  is correlated with an increase in the number of  $CuO_2$  planes per unit cell. Following the above arguments this makes sense in that it leads to more bands which produce more band crossings as shown schematically in Figure 9. For a three plane system we are now dealing with six bands. Four of these bands will be symmetric with respect to reflection through the middle plane (bands  $g1$ ,  $g2$ ,  $g3$ , and  $g4$ ) and two of these bands will be antisymmetric (bands  $u1$  and  $u2$ ). We argue that band repulsions near the  $(\pi/a, 0)$  point, as seen in the  $LASCO$  band structure, would be stronger for the  $g$  bands, since  $d_{z^2}$  character should appear in these bands at a higher energy than in the  $u$  bands. This could produce a crossing between the  $u1$  and  $g2$  bands at  $k_z = 0$  and  $k_z = \pi/c$  as depicted in the figure. Since the two surfaces might be expected to be highly coincident at this point, the number of thermally accessible crossing points should be high. Clearly, it can be seen that the addition of more  $CuO_2$  planes increases the probability of favorable crossing situations as illustrated here, and this should lead to potentially higher  $T_c$ ’s.

Finally we wish to note that the electron doped system,  $Nd_{2-x}Ce_xCuO_4$ ,<sup>18</sup> may be substantially different in regard to the nature of the two bands that cross. While we anticipate one of the bands will be “ $B_{1g}$ ”  $Cu$   $d_{x^2-y^2}$  in character, the other band is likely not “ $A_{1g}$ ”  $Cu$   $d_{z^2}$  since this band only appears as electrons are removed from the system. We suggest instead that the second band is a  $Nd/Ce$  band. It follows from this suggestion that high temperature superconductivity is not dependent on the specific crossing of the  $Cu$   $d_{x^2-y^2}$  and  $d_{z^2}$  bands. We stress, in fact, the only requirement of the IBP model that we now see is that some sort of crossing of bands occurs at the Fermi level. This leads us to be optimistic that with the careful exploitation of symmetry, entirely new classes of high temperature superconductors will be developed in our future.

## V. Conclusion.

We have presented the results of a new Hubbard model calculation on the optimally doped superconducting material  $La_{1.85}Sr_{0.15}CuO_4$ . We conclude from these calculations

that there is a crossing of two bands which occurs at the Fermi level. One of these bands is “ $B_{1g}$ ” in character, dominated by  $Cu\ d_{x^2-y^2}$  and the other is “ $A_{1g}$ ” in character, dominated by  $Cu\ d_{z^2}$ . The crossing rigorously occurs along the  $(0,0) - (\pi/a, \pi/a)$  symmetry line of the 2-D Brillouin zone. As detailed in the accompanying article by Tahir-Kheli,<sup>4</sup> an inter-band pairing (IBP) of electrons between these two bands leads to superconductivity. It can only occur at the critical doping level where the Fermi energy coincides with the band crossing, *i.e.*  $x = 0.15$ . The resulting density of states from this work is used in the accompanying work to explain a number of key experiments on this material.

Extension of the band model obtained for *LASCO* in these calculations to *YBCO* provides an easy explanation for the observation of a wide doping range for superconductivity to occur in this material as well as an explanation for the observation of two  $T_c$ ’s in different doping regimes. We anticipate at this point that other materials will be similarly understood largely through geometric considerations.

**Acknowledgment:** The authors wish to thank Dr. Jean-Marc Langlois for many useful discussions.

## References.

- <sup>1</sup> J.G. Bednorz and K.A. Müller, Z. Phys. B **64**, 189 (1986).
- <sup>2</sup> J. Tahir-Kheli, in *Proceedings of the 10th Anniversary HTS Workshop on Physics, Materials and Applications*, ed. B. Batlogg, C.W. Chu, W.K. Chu, D.U. Gubser, and K.A. Müller (World Scientific, New Jersey: 1996), 491-492.
- <sup>3</sup> H. Takagi, R.J. Cava, M. Marezio, B. Batlogg, J.J. Krajewski, W.F. Peck, Jr., P. Bordet, D.E. Cox, Phys. Rev. Lett. **68**, 3777 (1992).
- <sup>4</sup> J. Tahir-Kheli, <http://www.firstprinciples.com>, cond-mat/9711170
- <sup>5</sup> J.C. Slater, *Quantum Theory of Molecules and Solids, Vol. 4: The Self-Consistent Field for Molecules and Solids* (McGraw-Hill, New York, 1974); A. D. Becke, Phys. Rev. A **38**, 3098 (1988); C. Lee, W. Yang, and R. G. Parr, Phys. Rev. B **37**, 785 (1988); implemented as described in B. Miehlich, A. Savin, H. Stoll, and H. Preuss, Chem. Phys. Lett. **157**, 200 (1989).
- <sup>6</sup> W.J. Hehre and J.A. Pople, J. Chem. Phys. **56**, 4233 (1972).
- <sup>7</sup> P. J. Hay and W. R. Wadt, J. Chem. Phys. **82**, 299 (1985).
- <sup>8</sup> M. N. Ringnalda, J.-M. Langlois, R. B. Murphy, B. H. Greeley, C. Cortis, T. V. Russo, B. Marten, R. E. Donnelly, Jr., W. T. Pollard, Y. Cao, R. P. Muller, D. T. Mainz, J. R. Wright, G. H. Miller, W. A. Goddard III, and R. A. Friesner, Jaguar (formerly PS-GVB) v2.3, Schrödinger, Inc., 1996.
- <sup>9</sup> R.M. Hazen, in *Physical Properties of High Temperature Superconductors II*, ed. D.M. Ginsberg (World Scientific, New Jersey; 1990), 121-198.
- <sup>10</sup> J. Pipek and P. G. Mezey, J. Chem. Phys. **90**, 4916 (1989).
- <sup>11</sup> K. Shiraishi, A. Oshiyama, N. Shima, T. Nakayama, and H. Kamimura, Solid State Comm. **66**, 629 (1988).
- <sup>12</sup> A. Svane, Phys. Rev. Lett. **68**, 1900 (1992).
- <sup>13</sup> W.E. Pickett, Rev. Mod. Phys. **61**, 433 (1989), and references therein.
- <sup>14</sup> M. Eto, R. Saito, and H. Kamimura, Solid State Comm. **71**, 425 (1989).
- <sup>15</sup> R.J. Cava, B. Batlogg, C.H. Chen, E.A. Rietman, S.M. Zahurak, and D. Werder, Nature **329**, 423 (1987).
- <sup>16</sup> C. Michel, M. Hervieu, M.M. Borel, A. Grandin, F. Deslandes, J. Provost, and B. Raveau, Z. Phys. B **68** 421 (1987); H. Maeda, Y. Tanaka, M. Fukutomi, and T. Asano, Jpn. J. Appl. Phys. **27**, L209 (1988).
- <sup>17</sup> Z.Z. Sheng and A.M. Hermann, Nature **332**, 55 (1988); Z.Z. Sheng and A.M. Hermann **332**, 138 (1988).
- <sup>18</sup> Y. Tokura, H. Takagi, and S. Uchida, Nature **337**, 345 (1989).

**Table I.** Crystal structure of  $La_{1.85}Sr_{0.15}CuO_4$  (in Å).

$a$	3.788
$b$	3.788
$c$	13.206
$Cu$	(0.000,0.000,0.000)
$O(1)$	(0.500,0.000,0.000)
$O(2)$	(0.000,0.000,0.182)
$La/Sr$	(0.000,0.000,0.361)

**Table II.** Unscaled Hubbard parameters (in eV).  $E$  is an orbital energy,  $T$  an orbital coupling matrix element,  $J$  a Coulomb repulsion term, and  $K$  an exchange energy term.

$E(x^2 - y^2)$	-3.109	$J(x^2 - y^2/z^2)$	25.563	$K(x^2 - y^2/z^2)$	1.219
$E(z^2)$	-3.338	$J(x^2 - y^2/O p_\sigma)$	7.999	$K(x^2 - y^2/O p_\sigma)$	0.081
$E(O p_\sigma)$	-10.417	$J(x^2 - y^2/O2 p_z)$	6.471	$K(x^2 - y^2/O2 p_z)$	0.028
$E(O2 p_z)$	-12.442	$J(x^2 - y^2/O p_\pi)$	7.053	$K(x^2 - y^2/O p_\pi)$	0.006
$J(x^2 - y^2/x^2 - y^2)$	29.281	$J(z^2/O p_\sigma)$	6.471	$K(z^2/O p_\sigma)$	0.028
$J(z^2/z^2)$	25.990	$J(z^2/O2 p_z)$	6.855	$K(z^2/O2 p_z)$	0.262
$J(O p_\sigma/O p_\sigma)$	17.375	$J(z^2/O p_\pi)$	6.813	$K(z^2/O p_\pi)$	0.008
$J(O2 p_z/O2 p_z)$	11.365	$J(O p_\sigma/O p'_\sigma)$	5.345	$K(O p_\sigma/O p'_\sigma)$	0.035
$T(x^2 - y^2/O p_\sigma)$	1.347	$J(O p_\sigma/O p''_\sigma)$	3.890	$K(O p_\sigma/O p''_\sigma)$	0.008
$T(z^2/O p_\sigma)$	0.514	$J(O p_\sigma/O2 p_z)$	5.144	$K(O p_\sigma/O2 p_z)$	0.211
$T(z^2/O2 p_z)$	1.076	$J(O p_\sigma/O p_\pi)$	14.299	$K(O p_\sigma/O p_\pi)$	0.677
$T(O p_\sigma/O p'_\sigma)$	0.368	$J(O p_\sigma/O p'_\pi)$	5.548	$K(O p_\sigma/O p'_\pi)$	0.092
$T(O p_\sigma/O p''_\sigma)$	-0.041	$J(O p_\sigma/O p''_\pi)$	3.953	$K(O p_\sigma/O p''_\pi)$	0.008
$T(O p_\sigma/O2 p_z)$	0.078	$J(O2 p_z/O2 p'_z)$	3.502	$K(O2 p_z/O2 p'_z)$	0.098
$T(O2 p_z/O2 p'_z)$	0.493	$J(O2 p_z/O p_\pi)$	4.868	$K(O2 p_z/O p_\pi)$	0.087

**Table III.** Scaled Hubbard parameters (in eV).  $E$  is an orbital energy,  $T$  an orbital coupling matrix element,  $J$  a Coulomb repulsion term, and  $K$  an exchange energy term.

$E(x^2 - y^2)$	1.063	$J(x^2 - y^2/z^2)$	17.894	$K(x^2 - y^2/z^2)$	1.219
$E(z^2)$	0.596	$J(x^2 - y^2/O p_\sigma)$	5.599	$K(x^2 - y^2/O p_\sigma)$	0.081
$E(O p_\sigma)$	-10.071	$J(x^2 - y^2/O2 p_z)$	4.532	$K(x^2 - y^2/O2 p_z)$	0.028
$E(O2 p_z)$	-8.709	$J(x^2 - y^2/O p_\pi)$	4.937	$K(x^2 - y^2/O p_\pi)$	0.006
$J(x^2 - y^2/x^2 - y^2)$	20.497	$J(z^2/O p_\sigma)$	5.318	$K(z^2/O p_\sigma)$	0.028
$J(z^2/z^2)$	18.193	$J(z^2/O2 p_z)$	4.799	$K(z^2/O2 p_z)$	0.262
$J(O p_\sigma/O p_\sigma)$	12.163	$J(z^2/O p_\pi)$	4.769	$K(z^2/O p_\pi)$	0.008
$J(O2 p_z/O2 p_z)$	7.956	$J(O p_\sigma/O p'_\sigma)$	3.742	$K(O p_\sigma/O p'_\sigma)$	0.035
$T(x^2 - y^2/O p_\sigma)$	1.347	$J(O p_\sigma/O p''_\sigma)$	3.601	$K(O p_\sigma/O p''_\sigma)$	0.008
$T(z^2/O p_\sigma)$	0.514	$J(O p_\sigma/O2 p_z)$	3.601	$K(O p_\sigma/O2 p_z)$	0.211
$T(z^2/O2 p_z)$	1.076	$J(O p_\sigma/O p_\pi)$	10.009	$K(O p_\sigma/O p_\pi)$	0.677
$T(O p_\sigma/O p'_\sigma)$	0.368	$J(O p_\sigma/O p'_\pi)$	3.884	$K(O p_\sigma/O p'_\pi)$	0.092
$T(O p_\sigma/O p''_\sigma)$	-0.041	$J(O p_\sigma/O p''_\pi)$	2.767	$K(O p_\sigma/O p''_\pi)$	0.008
$T(O p_\sigma/O2 p_z)$	0.078	$J(O2 p_z/O2 p'_z)$	2.451	$K(O2 p_z/O2 p'_z)$	0.098
$T(O2 p_z/O2 p'_z)$	0.493	$J(O2 p_z/O p_\pi)$	3.408	$K(O2 p_z/O p_\pi)$	0.087

**Table IV.** Computed orbital energies and orbital occupations for optimally doped  $La_{1.85}Sr_{0.15}CuO_4$  taken from our Hubbard model using the scaled parameter set of Table III and no  $O p_\pi$  to  $La/Sr$  charge transfer. All energies are relative to the Fermi level (in eV).

Orbital	Energy	Occupation
$Cu x^2 - y^2$	-2.570	1.572
$Cu z^2$	-1.663	1.785
$O p_\sigma$	-4.254	1.806
$O2 p_z$	-1.611	1.941

**Table V.** Computed orbital energies and orbital occupations for optimally doped  $La_{1.85}Sr_{0.15}CuO_4$  taken from our Hubbard model using the scaled parameter set of Table III and 0.50 electron  $O$   $p_\pi$  to  $La/Sr$  charge transfer. All energies are relative to the Fermi level (in eV).

Orbital	Energy	Occupation
$Cu\ x^2 - y^2$	-2.403	1.770
$Cu\ z^2$	-2.092	1.666
$O\ p_\sigma$	-6.122	1.929
$O2\ p_z$	-0.852	1.777



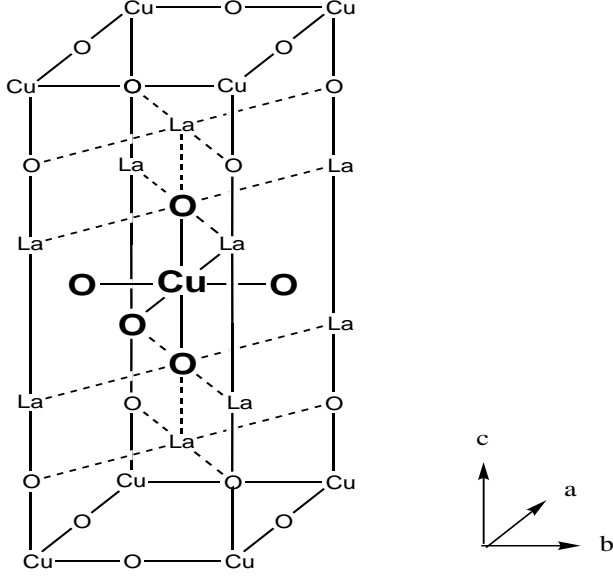


**FIG. 1.** Tetragonal unit cell of  $\text{La}_{1.85}\text{Sr}_{0.15}\text{CuO}_4$  showing the  $\text{CuO}_6$  cluster used in the DFT calculations in bold.

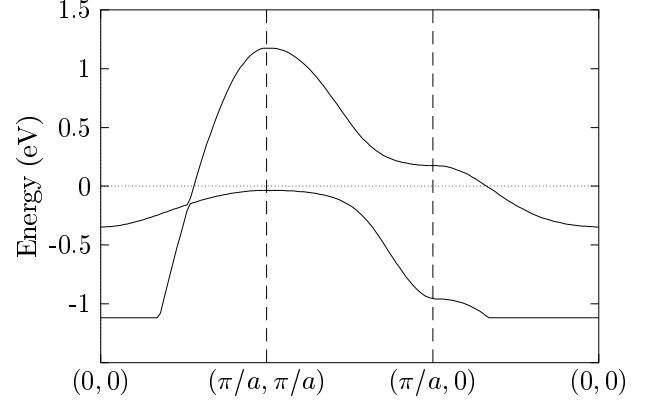


**FIG. 2.** Dispersion of the top two bands obtained from the Hubbard model using the scaled parameter set of Table III and no  $\text{O } p_\pi$  to La/Sr charge transfer, as shown along the symmetry line  $(0,0) - (\pi/a, \pi/a) - (\pi/a, 0) - (0,0)$ . The Fermi level is shown to lie just above the top of the lower band and only 0.153 eV above the crossing point along the  $(0,0) - (\pi/a, \pi/a)$  symmetry line.

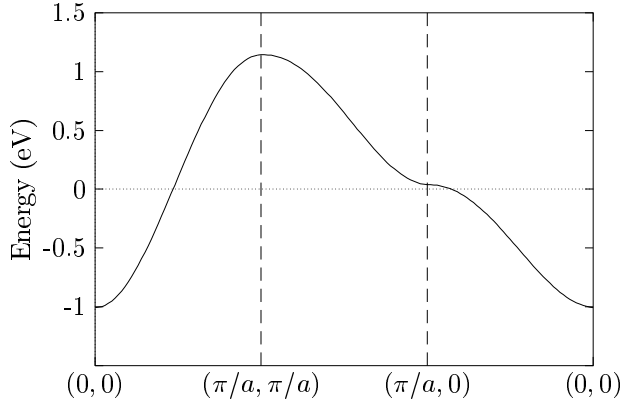


**FIG. 3.** Dispersion of the top band when the mean-field equation (3) is used in the Hubbard model (see description of Figure 2). Other bands are several eV lower in energy and are not shown.

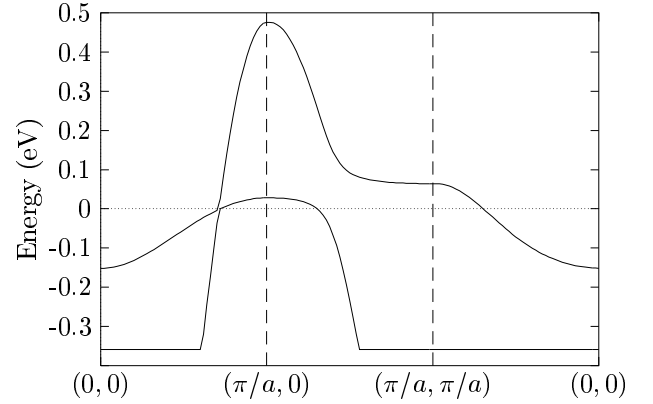


**FIG. 4.** Dispersion of the top two bands obtained from the Hubbard model using the scaled parameter set of Table III and 0.5 electron  $\text{O } p_\pi$  to La/Sr charge transfer, as shown along the symmetry lines  $(0,0) - (\pi/a, \pi/a) - (\pi/a, 0) - (0,0)$ . The Fermi level is shown to coincide with the crossing point along the  $(0,0) - (\pi/a, \pi/a)$  symmetry line.

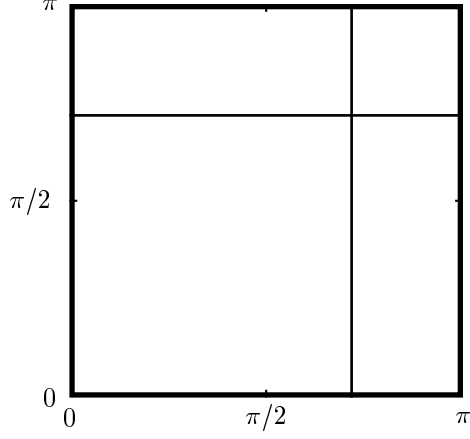


**FIG. 5.** Fermi surfaces showing the touching of the Upper and Lower bands along the  $(0, 0) - (\pi/a, \pi/a)$  symmetry line. The squareness of this surface is expected to change with the addition of longer range terms.

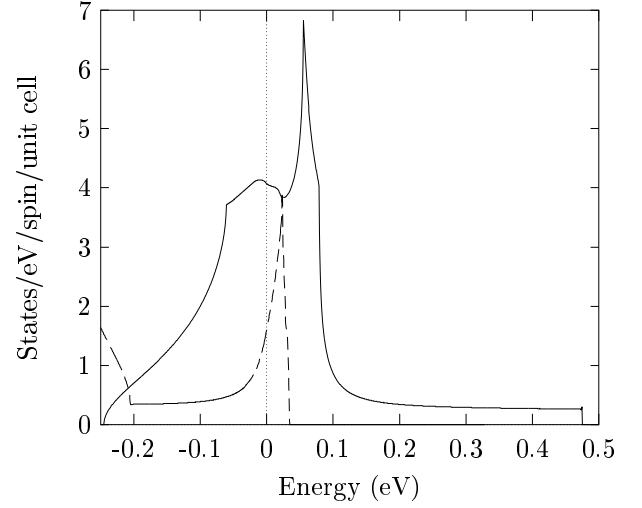


**FIG. 6.** Density of states of the top two bands shown from  $E = -0.25$  eV to  $E = +0.50$  eV.

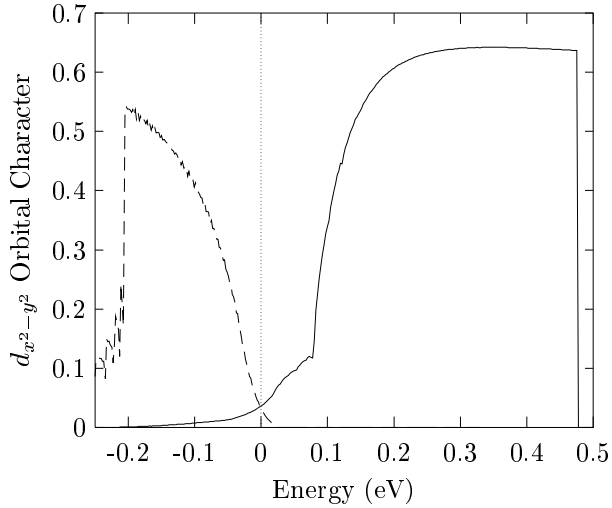


**FIG. 7a.** Extent of Cu  $d_{x^2-y^2}$  orbital character in the Upper (solid line) and Lower (dashed line) bands.

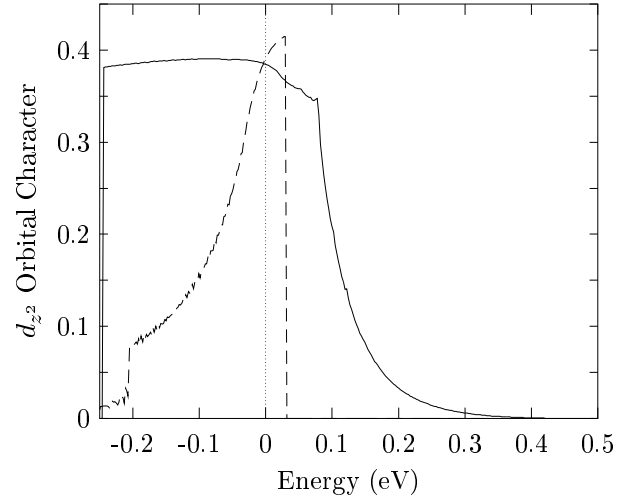


**FIG. 7b.** Extent of Cu  $d_{z^2}$  orbital character in the Upper (solid line) and Lower (dashed line) bands.

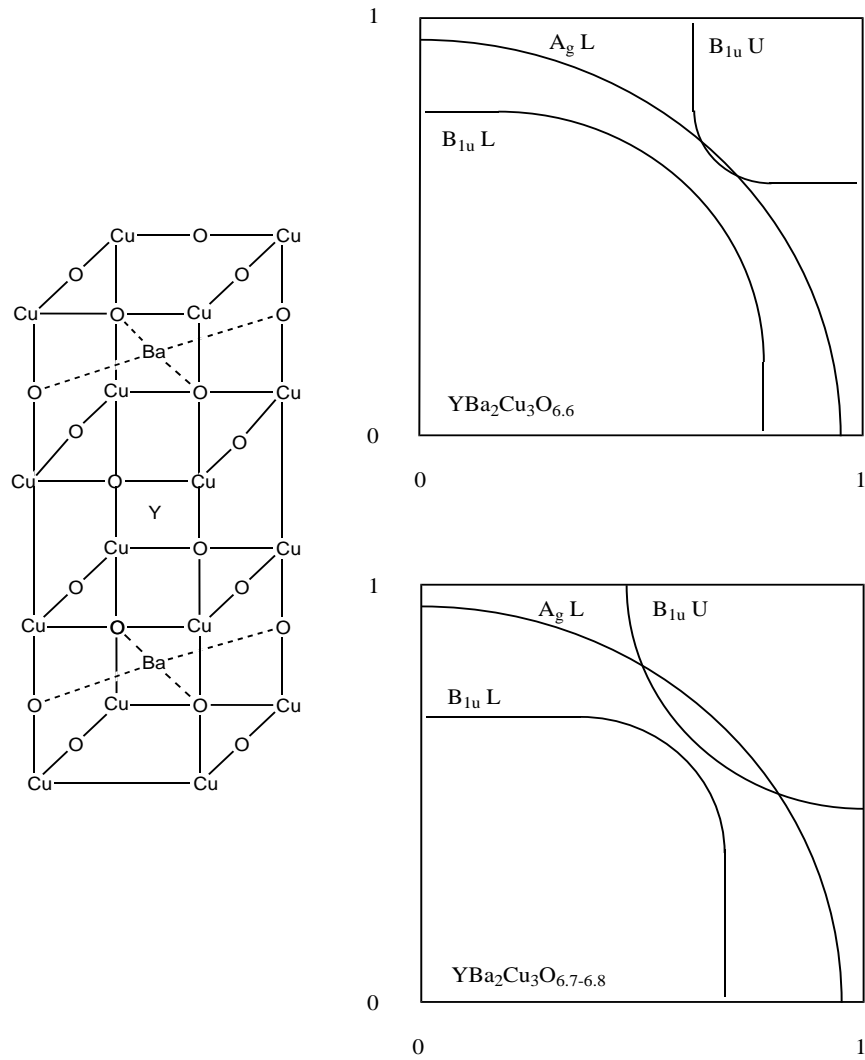


**FIG. 8.** Schematic depiction of Fermi surfaces for  $\text{YBa}_2\text{Cu}_3\text{O}_{6+\delta}$ . The onset of superconductivity is expected when the “ $B_{1u}$ ” L band and the “ $A_g$ ” L band first cross at  $k_z = \pi/c$  (top). Superconductivity continues upon further doping (bottom). A change in  $T_c$  may be expected when a similar set of crossing appears for  $k_z = 0$ . The YBCO unit cell is shown (left).

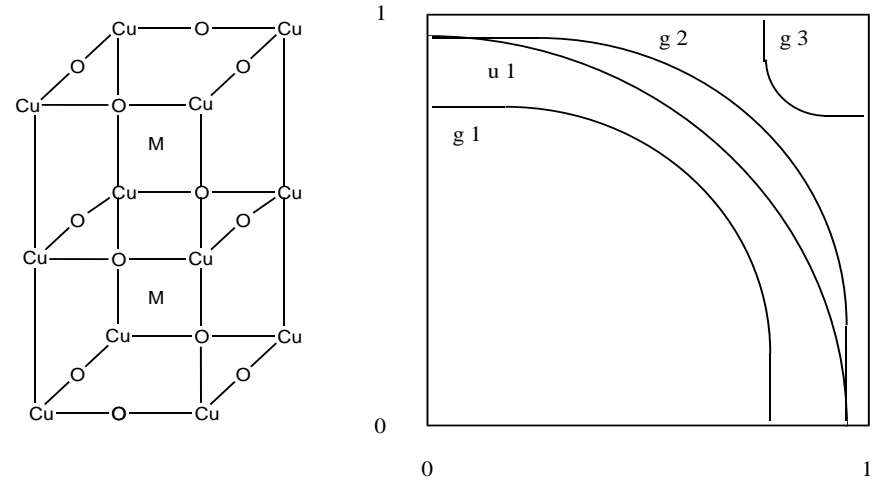


**FIG. 9.** Schematic depiction of Fermi surfaces for a typical 3-plane copper oxide superconductor. Band repulsions may lead to highly coincident  $g2$  and  $u1$  surfaces in the vicinity of  $(\pi/a, 0)$  when  $k_z = 0$  or  $k_z = \pi/c$ .